Drift-magnetohydrodynamical model of error-field penetration in tokamak plasmas

A. Cole and R. Fitzpatrick
Institute for Fusion Studies, Department of Physics, University of Texas at Austin, Austin, Texas 78712

(Received 16 September 2005; accepted 30 January 2006; published online 16 March 2006)

A previously published magnetohydrodynamical (MHD) model of error-field penetration in tokamak plasmas is extended to take drift-MHD physics into account. In particular, diamagnetic and semicollisional effects are both fully incorporated into the analysis. The new model is used to examine the scaling of the penetration threshold in ohmic tokamak plasmas. © *2006 American Institute of Physics*. [DOI: 10.1063/1.2178167]

I. INTRODUCTION

Tokamak plasmas are invariably subject to small amplitude, static, resonant magnetic perturbations—known as error fields—which are primarily generated by field-coil misalignments and uncompensated coil feeds. Error fields can drive magnetic reconnection, resulting in the formation of locked magnetic islands, in intrinsically tearing-stable plasmas. Ohmic tokamak plasmas containing locked islands are found to be exceptionally disruption prone. Fortunately, error-field driven reconnection is strongly suppressed by the naturally occurring mode rotation in ohmic plasmas. However, when the error-field amplitude rises above a certain critical value, the rotation is suddenly arrested, and error-field driven reconnection proceeds unhindered. This phenomenon is known as error-field penetration. The scenario outlined above has been observed in a number of tokamak experiments.[1–6]

A model of error-field penetration has been developed which is based on the premise that, prior to penetration, the rotational suppression of error-field driven reconnection is sufficiently strong that the plasma response is governed by linear layer physics.[7–9] This model seems to offer a coherent explanation for the various experimental signatures of error-field penetration, i.e. (i) the sudden appearance of a magnetic signal on the locked-mode detector, with no rotating precursor detected on the Mirnov coils; (ii) a simultaneous marked reduction in the core plasma rotation; (iii) a simultaneous degradation in the plasma confinement; (iv) a strong dependence of the penetration threshold on the amplitudes of the resonant components of the error field, and a lack of dependence on the amplitudes of the nonresonant components; and (v) a reproducible threshold given the same plasma equilibrium and the same error field. However, the model in question is based on a magnetohydrodynamical (MHD) treatment of the plasma. Strictly speaking, such a treatment is invalid (even in ohmic discharges) in the high temperature plasmas which occur in present-day tokamak experiments. As is well-known, high temperature plasmas are far better modeled using the drift-MHD[10] ordering. Hence, the aim of this paper is to develop a drift-MHD version of the aforementioned model of error-field penetration.

The principal modifications to MHD which arise in drift-MHD theory are the appearance of diamagnetic flows, in addition to $\mathbf{E}\times\mathbf{B}$ flow, and the decoupling of the ion and electron fluids on length scales below ρ_s (the ion Larmor radius calculated with the electron temperature). We, therefore, wish to investigate whether the error-field penetration threshold is substantially modified if the intrinsic mode rotation is largely diamagnetic in nature (as may well be the case in ohmic tokamak plasmas) instead of being solely due to $\mathbf{E}\times\mathbf{B}$ flow. We also wish to examine to what extent the threshold changes when the reconnecting layer width falls below ρ_s, and enters the so-called semicollisional regime[11,12] (as is likely to occur in large ohmic tokamak plasmas).

This paper is organized as follows. In Sec. II, working in slab geometry, we derive the fundamental force balance equation which controls error-field penetration. In Sec. III, again working in slab geometry, we solve the equations which control the response of the reconnecting layer to the applied error field, and catalog all of the possible drift-MHD response regimes. In Sec. IV, we apply the slab analysis outlined in Secs. II and III to the problem of determining the error-field penetration threshold in ohmic tokamak plasmas, and then investigate the scaling of the penetration threshold thus obtained.

II. DERIVATION OF FORCE BALANCE EQUATION

A. Basic equations

Standard right-handed Cartesian coordinates (x,y,z) are adopted. Consider a quasineutral plasma with singly charged ions of mass m_i. The ion/electron number density n_e is assumed to be uniform and constant. Suppose that $T_i=\tau T_e$, where $T_{i,e}$ is the ion/electron temperature, and τ is uniform and constant. Let there be no variation of quantities in the z direction, i.e., $\partial/\partial z\equiv 0$. Finally, let all lengths be normalized to some convenient scale length l, all magnetic field strengths to some convenient scale field strength B_l, and all times to $t_l\equiv l/V_l$, where $V_l=B_l/\sqrt{\mu_0 n_e m_i}$.

We can write $\mathbf{B}=\nabla\psi\times\hat{\mathbf{z}}+(B_0+b_z)\hat{\mathbf{z}}$, and $P=P_0-B_0 b_z+O(1)$, where $\mathbf{B}$ is the magnetic field, and P the total plasma pressure. Here, we are assuming that P_0 and B_0 are uniform, and $P_0\gg B_0\gg 1$, with ψ and b_z both $O(1)$.[13] Let $\beta=\Gamma P_0/B_0^2$ be (Γ times) the plasma beta calculated with the "guide field," B_0, where $\Gamma=5/3$ is the plasma ratio of specific heats. Note that the above ordering scheme (which in tokamak ter-

minology is a high poloidal beta ordering scheme) does not constrain β (which in tokamak terminology is the toroidal beta) to be either much less than or much greater than unity.

We adopt the reduced, two-dimensional (2D), drift-MHD equations derived in Ref. 13,

$$\frac{\partial \psi}{\partial t} = [\phi - Z, \psi] + \eta J, \tag{1}$$

$$\frac{\partial Z}{\partial t} = [\phi, Z] + c_\beta^2 [V_z, \psi] + d_\beta^2 [J, \psi] + c_\beta^2 \eta Y, \tag{2}$$

$$\frac{\partial U}{\partial t} = [\phi, U] - \frac{\tau}{2}\{\nabla^2[\phi, Z] + [U, Z] + [Y, \phi]\} + [J, \psi] + \mu_i \nabla^2 (U + \tau Y), \tag{3}$$

$$\frac{\partial V_z}{\partial t} = [\phi, V_z] + [Z, \psi] + \mu_i \nabla^2 V_z, \tag{4}$$

where $J = 1 + \nabla^2 \psi$, $U = \nabla^2 \phi$, and $Y = \nabla^2 Z$. Here, $c_\beta = \sqrt{\beta/(1+\beta)}$, $d_\beta = c_\beta d_i/\sqrt{1+\tau}$, $Z = d_i b_z/(1+\tau)$, $d_i = (m_i/n_e e^2 \mu_0)^{1/2}/l$, and $[A, B] = \nabla A \times \nabla B \cdot \hat{\mathbf{z}}$. The guiding-center velocity is written $\mathbf{V} = \nabla \phi \times \hat{\mathbf{z}} + d_i (c_\beta/d_\beta)^2 V_z \hat{\mathbf{z}}$. Moreover, η is the (uniform) plasma resistivity, μ_i the (uniform) ion viscosity, and d_i the normalized collisionless ion skin depth. Finally, ψ is the magnetic flux function, Z is proportional to the perturbed plasma pressure, ϕ is the guiding-center stream function, and V_z is the (normalized) ion velocity in the z direction.

Note that, in adapting the above equations from Ref. 13, we have neglected electron viscosity and thermal conductivity, for the sake of simplicity. Note also that the transport coefficient μ_i, appearing in these equations, is phenomenological in nature, and is supposed to represent the anomalous transport of momentum across magnetic flux surfaces due to small-scale plasma turbulence. Equations (1)–(4) contain both electron and ion diamagnetic effects, including the contribution of the anisotropic ion gyroviscous tensor, but neglect electron inertia. Our equations are "reduced" in the sense that they do not contain the compressible Alfvén wave. However, they do contain the shear-Alfvén wave, the magnetoacoustic wave, and the whistler/kinetic-Alfvén wave.

B. Initial plasma equilibrium

Suppose that the plasma is periodic in the y direction, with period L, and is bounded by perfectly conducting walls at $x = \pm 1$. The initial plasma equilibrium takes the form $\psi^{(0)}(x) = -x^2/2$, $Z^{(0)}(x) = -V_* x/(1+\tau)$, $\phi^{(0)}(x) = -V_0 x$, and $U^{(0)}(x) = V_z^{(0)}(x) = 0$. This is a tearing-stable equilibrium, with the uniform y-directed $\mathbf{E} \times \mathbf{B}$ velocity V_0, and the uniform y-directed ion and electron diamagnetic velocities $V_{*i} = \tau V_*/(1+\tau)$ and $V_{*e} = -V_*/(1+\tau)$, respectively. Here, $V_* \equiv V_{*i} - V_{*e}$ is the total diamagnetic velocity.

C. Error field

The error field is generated by applying equal and opposite, x-directed, periodic displacements, $\Xi(t)\sin(ky)$, to the conducting walls, where $k = 2\pi/L$. The appropriate boundary condition on ψ is simply

$$\psi(\pm 1, y, t) = -\frac{1}{2} + \Xi(t)\sin(ky). \tag{5}$$

In the following, $\Xi(t)$ is assumed to be either static, or very slowly varying, as is appropriate for an error field.

D. Asymptotic matching

Throughout most of the plasma, the response to the applied error field is determined by the equations of marginally stable, ideal-MHD.[14] This region is termed the outer region. Marginally stable, ideal-MHD breaks down in a thin layer, centered on $x = 0$, which is termed the inner region.

In the outer region, the vorticity equation. (3) reduces to $[\nabla^2 \psi, \psi] \simeq 0$. Linearizing this equation, assuming a $\sin(ky)$ dependence of perturbed quantities in the y direction, we obtain

$$\frac{\partial^2 \tilde{\psi}}{\partial x^2} - k^2 \tilde{\psi} \simeq 0 \tag{6}$$

in the outer region, where $\sim$ denotes a perturbed quantity. The boundary conditions are $\tilde{\psi}(-x, t) = \tilde{\psi}(x, t)$, from symmetry, and $\tilde{\psi}(\pm 1, t) = \Xi(t)$. The most general solution to Eq. (6) takes the form

$$\tilde{\psi}(x, t) = \Psi(t)\left(\cosh kx - \frac{\sinh k|x|}{\tanh k}\right) + \Xi(t)\frac{\sinh k|x|}{\sinh k}, \tag{7}$$

where $\Psi(t)$ is the perturbed magnetic flux at the edge of the inner region (which equals the reconnected flux in a constant-ψ regime). The parameter

$$\Delta = \left[\frac{\partial \ln \psi}{\partial x}\right]_{0-}^{0+} \tag{8}$$

measures the strength of the current sheet induced in the inner region. Asymptotic matching between the inner and outer regions yields

$$\Psi(t) = \frac{E_{sw}\Xi(t)}{(-E_{ss}) + \Delta(t)}, \tag{9}$$

where $E_{ss} = -2k/\tanh k$, and $E_{sw} = 2k/\sinh k$. Note that $E_{ss} < 0$ is the conventional tearing stability index.[14]

E. Electromagnetic force

The mean electromagnetic force (density) acting on the plasma in the y direction takes the form

$$f_y = -\frac{k}{2}\,\mathrm{Im}\left(\frac{\partial^2 \tilde{\psi}}{\partial x^2}\tilde{\psi}^*\right). \tag{10}$$

It is clear, from Eq. (6), that zero mean force is exerted on the plasma in the outer region. The net mean force exerted on the inner region is written

$$F_{EMy} = \int_{0-}^{0+} f_y \, dx = -\frac{k}{2} \, \mathrm{Im}(\Delta)|\Psi|^2. \tag{11}$$

F. Modified E×B velocity profile

Now, we do not expect the applied error field to significantly change the equilibrium electron/ion diamagnetic velocity profiles, i.e., we do not expect a change in the equilibrium plasma pressure gradient. However, the error field is free to modify the equilibrium $\mathbf{E}\times\mathbf{B}$ velocity profile (by exerting electromagnetic forces on the plasma). In fact, the steady-state perturbed velocity profile takes the form

$$V_y^{(0)\prime}(x) = V_0 + (V - V_0)(1 - |x|), \tag{12}$$

where V is the modified $\mathbf{E}\times\mathbf{B}$ velocity at $x=0$. The above velocity profile is consistent with an error-field induced electromagnetic force which is localized around $x=0$, and boundary conditions which effectively prevent the equilibrium electric field at the edge of the plasma from changing.[7]

G. Viscous force

The net y-directed viscous force acting on the inner region in a steady state is given by

$$F_{VSy} = \mu_i \left[\frac{dV_y^{(0)\prime}}{dx} \right]_{0-}^{0+} = 2\mu_i (V_0 - V). \tag{13}$$

H. Force balance

In a steady state, zero net force acts on the inner region in the y direction. It follows that

$$F_{EMy} + F_{VSy} = 0, \tag{14}$$

or

$$\frac{k}{2}(E_{sw}\Xi)^2 \frac{\mathrm{Im}(\Delta)}{|(-E_{ss}) + \Delta|^2} = 2\mu_i (V_0 - V). \tag{15}$$

I. Normalized force balance equation

Let $Q=(k/\eta)^{1/3}V$, $Q_0=(k/\eta)^{1/3}V_0$, $\hat{\Delta}=(\eta/k)^{1/3}\Delta$, $\xi=(k/\eta)^{1/2}E_{sw}\Xi$, $\alpha=(\eta/k)^{1/3}(-E_{ss})$, and $P=\mu_i/\eta$. The normalized force balance equation becomes

$$\frac{\mathrm{Im}[\hat{\Delta}(Q)]}{|\alpha + \hat{\Delta}(Q)|^2} = \frac{4P(Q_0 - Q)}{\xi^2}. \tag{16}$$

To make further progress, we need to evaluate $\hat{\Delta}(Q)$. This information can only be obtained from nonideal layer physics.

III. DRIFT-MHD LAYER PHYSICS

A. Introduction

Suppose that the error field is quasistatic, so that $\Xi(t) \simeq \Xi_0$. Linearizing Eqs. (1)–(4), assuming an $\exp(iky)$ dependence of perturbed quantities in the y direction, normalizing, and taking the limits $\partial/\partial t=0$ and $|x| \ll 1$, we obtain

$$i(Q - Q_e)\tilde{\psi} = iX(\tilde{\phi} - \tilde{Z}) + \frac{d^2\tilde{\psi}}{dX^2}, \tag{17}$$

$$iQ\tilde{Z} = iQ_e\tilde{\phi} + iD^2X\frac{d^2\tilde{\psi}}{dX^2} + ic_\beta^2 X\tilde{V}_z + c_\beta^2\frac{d^2\tilde{Z}}{dX^2}, \tag{18}$$

$$i(Q - Q_i)\frac{d^2\tilde{\phi}}{dX^2} = iX\frac{d^2\tilde{\psi}}{dX^2} + P\frac{d^4(\tilde{\phi} + \tau\tilde{Z})}{dX^4}, \tag{19}$$

$$iQ\tilde{V}_z = -iQ_e\tilde{\psi} + iX\tilde{Z} + P\frac{d^2\tilde{V}_z}{dX^2}, \tag{20}$$

where $X=(k/\eta)^{1/3}x$, $D=(k/\eta)^{1/3}d_\beta$, and $Q_{i,e}=-(k/\eta)^{1/3}V_{*i,e}$. Asymptotic matching to the outer region yields the boundary condition [see Eqs. (7) and (8)]

$$\tilde{\psi}(X) \to \Psi\left[1 + \frac{\hat{\Delta}}{2}|X| + O(X^2)\right] \tag{21}$$

as $|X| \to \infty$.

B. Fourier transformation

Let

$$\bar{\phi}(p) = \int_{-\infty}^{\infty} \tilde{\phi}(X) e^{+ipX} dX, \tag{22}$$

etc. The Fourier transformed layer equations become

$$i(Q - Q_e)\bar{\psi} = \frac{d(\bar{\phi} - \bar{Z})}{dp} - p^2\bar{\psi}, \tag{23}$$

$$iQ\bar{Z} = iQ_e\bar{\phi} - D^2\frac{d(p^2\bar{\psi})}{dp} + c_\beta^2\frac{d\bar{V}_z}{dp} - c_\beta^2 p^2\bar{Z}, \tag{24}$$

$$i(Q - Q_i)p^2\bar{\phi} = \frac{d(p^2\bar{\psi})}{dp} - Pp^4(\bar{\phi} + \tau\bar{Z}), \tag{25}$$

$$iQ\bar{V}_z = -iQ_e\bar{\psi} + \frac{d\bar{Z}}{dp} - Pp^2\bar{V}_z, \tag{26}$$

where

$$\bar{\phi}(p) \to \bar{\phi}_0\left[\frac{\hat{\Delta}}{\pi}\frac{1}{p} + 1 + O(p)\right] \tag{27}$$

as $p \to 0$.

C. Layer equation

Let us ignore the term $c_\beta^2 d\bar{V}_z/dp$ in Eq. (24). This approximation can be verified *a posteriori*. Equations (23)–(26) reduce to

$$\frac{d}{dp}\left[\frac{p^2}{i(Q-Q_e)+p^2}\frac{dY}{dp}\right] - \left[\frac{-Q(Q-Q_i)+i(Q-Q_i)(P+c_\beta^2)p^2+c_\beta^2 P p^4}{i(Q-Q_e)+\{c_\beta^2+i(Q-Q_i)D^2\}p^2+(1+\tau)PD^2p^4}\right] \times p^2 Y = 0, \tag{28}$$

where

$$Y = \left[\frac{i(Q-Q_e)+\{c_\beta^2+i(Q-Q_i)D^2\}p^2+(1+\tau)PD^2p^4}{iQ+c_\beta^2p^2+\tau PD^2p^4}\right]\bar{\phi}. \tag{29}$$

The boundary conditions are that $Y(p)$ is bounded as $p\to\infty$, and

$$Y(p)\to Y_0\left[\frac{\hat{\Delta}}{\pi p}+1+O(p)\right] \tag{30}$$

as $p\to 0$. This is sufficient to uniquely determine $\hat{\Delta}(Q)$. In general, we can find analytic solutions to Eq. (28), which are well-behaved as $p\to\infty$, and satisfy Eq. (30) as $p\to 0$, by one of two different methods. The first method, outlined in Sec. III D, is a two-step matching process that generates a class of solutions which satisfies the constant-ψ approximation.[14] The second method, outlined in Sec. III F, is a one-step matching process that generates a class of *nonconstant-ψ* solutions. In the following, we assume that $|Q-Q_e|\sim|Q-Q_i|\sim|Q|$, and $\tau\sim O(1)$, for the sake of simplicity.

D. Constant-ψ approximation

Let there be two layers in p space. In the small-p layer, suppose that Eq. (28) reduces to

$$\frac{d}{dp}\left(\frac{p^2}{i(Q-Q_e)+p^2}\frac{dY}{dp}\right)\simeq 0 \tag{31}$$

when $p\sim Q^{1/2}$. Integrating directly, we find

$$Y(p)\simeq Y_0\left[\frac{\hat{\Delta}}{\pi}\left(\frac{1}{p}-\frac{p}{i(Q-Q_e)}\right)+1+O(p^2)\right] \tag{32}$$

for $p\lesssim O(Q^{1/2})$. This approximation, which is equivalent to the well-known constant-ψ approximation,[14] is valid provided

$$\frac{Q^3(1+P)}{1+D^2Q(1+P)}\ll 1. \tag{33}$$

In the large-p layer, for $p\gg Q^{1/2}$, we obtain

$$\frac{d^2Y}{dp^2} - \left[\frac{-Q(Q-Q_i)+i(Q-Q_i)(P+c_\beta^2)p^2+c_\beta^2 P p^4}{i(Q-Q_e)+\{c_\beta^2+i(Q-Q_i)D^2\}p^2+(1+\tau)PD^2p^4}\right] \times p^2 Y \simeq 0, \tag{34}$$

with $Y(p)$ bounded as $p\to\infty$. Asymptotic matching to the small-p layer yields the boundary condition

$$Y(p)\simeq Y_0\left[1-\frac{\hat{\Delta}}{\pi i(Q-Q_e)}p+O(p^2)\right] \tag{35}$$

as $p\to 0$.

In the various constant-ψ regimes considered below, Eq. (34) reduces to an equation of the form

$$\frac{d^2Y}{dp^2}-Cp^mY\simeq 0, \tag{36}$$

where m is real and non-negative, and C is some complex constant. Let $Y=\sqrt{p}G$ and $z=\sqrt{C}p^n/n$, where $n=(m+2)/2$. The above equation transforms into a modified Bessel equation of general order,

$$z^2\frac{d^2G}{dz^2}+z\frac{dG}{dz}-(z^2+\nu^2)G=0, \tag{37}$$

with $\nu=1/(m+2)$. The solution which is bounded as $z\to\infty$ has the small-z expansion[15]

$$K_\nu(z)=\frac{1}{\Gamma(1-\nu)}\left(\frac{2}{z}\right)^\nu-\frac{1}{\Gamma(1+\nu)}\left(\frac{z}{2}\right)^\nu+O(z^{2-\nu}). \tag{38}$$

A comparison of the above expression with Eq. (35) yields

$$\hat{\Delta}=\pi i(Q-Q_e)\frac{\Gamma(1-\nu)}{\Gamma(\nu)}\nu^{2\nu-1}C^\nu. \tag{39}$$

Note, finally, that $p_*\sim C^{-\nu}$, where p_* denotes the width of the large-p layer in p space.

E. Constant-ψ regimes

Suppose that $Q\gg c_\beta^2p^2$ and $Q\gg Pp^2$. Equation (34) reduces to

$$\frac{d^2Y}{dp^2}-\left[\frac{iQ(Q-Q_i)}{(Q-Q_e)+(Q-Q_i)D^2p^2}\right]p^2Y\simeq 0. \tag{40}$$

In the limit $1\gg D^2p^2$, Eqs. (36), (39), and (40) yield

$$\hat{\Delta}(Q)=\frac{2\pi\Gamma(3/4)}{\Gamma(1/4)}(iQ)^{1/4}[i(Q-Q_i)]^{1/4}[i(Q-Q_e)]^{3/4}. \tag{41}$$

We shall refer to this as the first resistive-inertial (RIi) regime,[8,14,16] since the plasma response is dominated by resistivity and ion inertia. In the limit $1\ll D^2p^2$, (36), (39), and (40) give

$$\hat{\Delta}(Q)=\pi\frac{(iQ)^{1/2}[i(Q-Q_e)]}{D}. \tag{42}$$

We shall refer to this as the second semicollisional (SCii) regime.

Suppose that $Q\ll c_\beta^2p^2$ and $Q\gg Pp^2$. Equation (34) reduces to

$$\frac{d^2Y}{dp^2}-\frac{i(Q-Q_i)c_\beta^2p^2}{c_\beta^2+i(Q-Q_i)D^2}Y\simeq 0. \tag{43}$$

In the limit $Q\ll(c_\beta/D)^2$, Eqs. (36), (39), and (43) yield

$$\hat{\Delta}(Q) = \frac{2\pi\Gamma(3/4)}{\Gamma(1/4)}[i(Q-Q_i)]^{1/4}[i(Q-Q_e)]. \tag{44}$$

We shall refer to this as the second resistive-inertial (RIii) regime. In the limit $Q \gg (c_\beta/D)^2$, Eqs. (36), (39), and (43) give

$$\hat{\Delta}(Q) = \frac{2\pi\Gamma(3/4)}{\Gamma(1/4)}[i(Q-Q_e)]\frac{c_\beta^{1/2}}{D^{1/2}}. \tag{45}$$

We shall refer to this as the second Hall-resistive (HRii) regime, since the plasma response is dominated by resistivity and the Hall term.

Suppose that $Q \gg c_\beta^2 p^2$ and $Q \ll P p^2$. Equation (34) reduces to

$$\frac{d^2Y}{dp^2} - \frac{i(Q-Q_i)Pp^4}{i(Q-Q_e)+(1+\tau)PD^2p^4}Y \simeq 0. \tag{46}$$

In the limit $Q \gg PD^2p^4$, Eqs. (36), (39), and (46) yield

$$\hat{\Delta}(Q) = \frac{6^{2/3}\pi\Gamma(5/6)}{\Gamma(1/6)}[i(Q-Q_i)]^{1/6}[i(Q-Q_e)]^{5/6}P^{1/6}. \tag{47}$$

We shall refer to this as the first visco-resistive (VRi) regime,[8] since the plasma response is dominated by viscosity and resistivity. In the limit $Q \ll PD^2p^4$, Eqs. (36), (39), and (46) give

$$\hat{\Delta}(Q) = \pi\frac{[i(Q-Q_i)]^{1/2}[i(Q-Q_e)]}{D\sqrt{1+\tau}}. \tag{48}$$

We shall refer to this as the first semicollisional (SCi) regime.[11,12]

Suppose that $Q \ll c_\beta^2 p^2$ and $Q \ll P p^2$. Equation (34) reduces to

$$\frac{d^2Y}{dp^2} - \frac{c_\beta^2 Pp^4}{c_\beta^2+(1+\tau)PD^2p^2}Y \simeq 0. \tag{49}$$

In the limit $c_\beta^2 \gg PD^2p^2$, Eqs. (36), (39), and (49) yield

$$\hat{\Delta}(Q) = \frac{6^{2/3}\pi\Gamma(5/6)}{\Gamma(1/6)}[i(Q-Q_e)]P^{1/6}. \tag{50}$$

We shall refer to this as the second visco-resistive (VRii) regime. Finally, in the limit $c_\beta^2 \ll PD^2p^2$, Eqs. (36), (39), and (49) give

$$\hat{\Delta}(Q) = \frac{2\pi\Gamma(3/4)}{\Gamma(1/4)}[i(Q-Q_e)]\frac{c_\beta^{1/2}}{(1+\tau)^{1/4}D^{1/2}}. \tag{51}$$

We shall refer to this as the first Hall-resistive (HRi) regime.

F. Nonconstant-ψ regimes

Suppose that $p \ll Q^{1/2}$. In this limit, Eq. (28) yields

$$\frac{d}{dp}\left(p^2\frac{dY}{dp}\right) - \left[\frac{i(Q-Q_e)\{-Q(Q-Q_i)+i(Q-Q_i)(P+c_\beta^2)p^2+c_\beta^2Pp^4\}}{i(Q-Q_e)+\{c_\beta^2+i(Q-Q_i)D^2\}p^2+(1+\tau)PD^2p^4}\right]p^2Y \simeq 0. \tag{52}$$

In the various nonconstant-ψ regimes considered below, Eq. (52) reduces to

$$\frac{d}{dp}\left(p^2\frac{dY}{dp}\right) - Cp^{m+2}Y \simeq 0, \tag{53}$$

where m is real and non-negative, and C is a complex constant. Let $G=pY$. The above equation transforms to

$$\frac{d^2G}{dp^2} - Cp^mG \simeq 0. \tag{54}$$

This equation is identical in form to Eq. (36), which we have already solved. Indeed, the solution which is bounded as $p \to \infty$ has the small-p expansion (38), where $z=\sqrt{C}p^n/n$, and $n=(m+2)/2$. The layer width in p space again scales as $p_* \sim C^{-\nu}$. Matching to Eq. (30) yields

$$\hat{\Delta} = -\pi\frac{\Gamma(\nu)}{\Gamma(1-\nu)}\nu^{1-2\nu}C^{-\nu}, \tag{55}$$

where $\nu=1/(m+2)$.

Suppose that $Q \gg c_\beta^2p^2, QD^2p^2, PD^2p^4$. Equation (52) reduces to

$$\frac{d^2G}{dp^2} - i(Q-Q_i)(iQ+Pp^2)G \simeq 0. \tag{56}$$

In the limit $Q \ll Pp^2$, Eqs. (53), (55), and (56) give

$$\hat{\Delta}(Q) = -\frac{\pi}{2}\frac{\Gamma(1/4)}{\Gamma(3/4)}[i(Q-Q_i)]^{-1/4}P^{-1/4}. \tag{57}$$

We shall refer to this as the visco-inertial (VI) regime,[8] since the plasma response is dominated by viscosity and ion inertia. In the limit $Q \gg Pp^2$, Eqs. (53), (55), and (56) yield

$$\hat{\Delta}(Q) = -\frac{\pi}{(iQ)^{1/2}[i(Q-Q_i)]^{1/2}}. \tag{58}$$

We shall refer to this as the inertial (I) regime,[8,16] since the plasma response is dominated by ion inertia. Note that the plasma response in the inertial regime is equivalent to that of two closely spaced Alfvén resonances which straddle the resonant surface.[17]

TABLE I. Linear drift-MHD response regimes for a static error field. The abbreviations indicate the various different response regimes: HRi—first Hall-resistive; HRii—second Hall-resistive; SCi—first semicollisional; SCii—second semicollisional; RIi—first resistive-inertial; RIii—second resistive-inertial; VRi—first visco-resistive; VRii—second visco-resistive; VI—visco-inertial; I—inertial. Here, $\hat{\Delta}=(\eta/k)^{1/3}\Delta$, $Q=(k/\eta)^{1/3}V$, $Q_{i,e}=-(k/\eta)^{1/3}V_{*i,e}$, $D=(k/\eta)^{1/3}d_\beta$, and $P=\mu_i/\eta$.

Abbreviation	Response	Layer width, p_*
HRi	$\hat{\Delta}=2.124[i(Q-Q_e)]c_\beta^{1/2}D^{-1/2}(1+\tau)^{-1/4}$	$D^{1/2}c_\beta^{-1/2}$
HRii	$\hat{\Delta}=2.124[i(Q-Q_e)]c_\beta^{1/2}D^{-1/2}$	$D^{1/2}c_\beta^{-1/2}$
SCi	$\hat{\Delta}=3.142[i(Q-Q_i)]^{1/2}[i(Q-Q_e)]D^{-1}(1+\tau)^{-1/2}$	$DQ^{-1/2}$
SCii	$\hat{\Delta}=3.142(iQ)^{1/2}[i(Q-Q_e)]D^{-1}$	$DQ^{-1/2}$
RIi	$\hat{\Delta}=2.124(iQ)^{1/4}[i(Q-Q_i)]^{1/4}[i(Q-Q_e)]^{3/4}$	$Q^{-1/4}$
RIii	$\hat{\Delta}=2.124[i(Q-Q_i)]^{1/4}[i(Q-Q_e)]$	$Q^{-1/4}$
VRi	$\hat{\Delta}=2.104[i(Q-Q_i)]^{1/6}[i(Q-Q_e)]^{5/6}P^{1/6}$	$P^{-1/6}$
VRii	$\hat{\Delta}=2.104[i(Q-Q_e)]P^{1/6}$	$P^{-1/6}$
VI	$\hat{\Delta}=-4.647[i(Q-Q_i)]^{-1/4}P^{-1/4}$	$Q^{-1/4}P^{-1/4}$
I	$\hat{\Delta}=-3.142(iQ)^{-1/2}[i(Q-Q_i)]^{-1/2}$	Q^{-1}

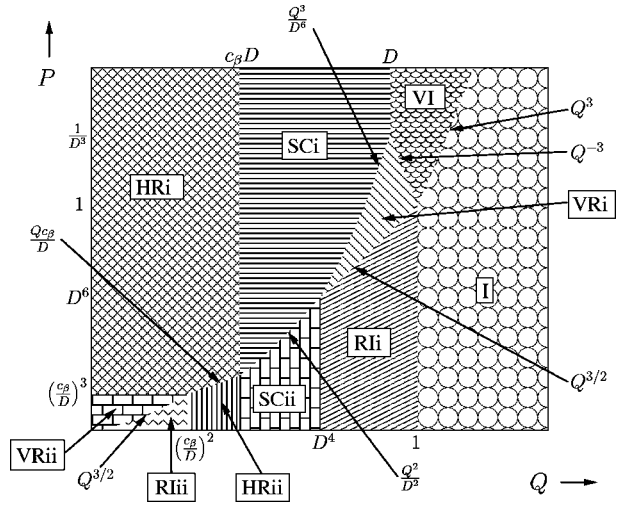

FIG. 2. A schematic diagram of the linear drift-MHD response regimes in Q–P space for the case $c_\beta^{1/3}\ll D\ll 1$. Here, $Q=(k/\eta)^{1/3}V$, $P=\mu_i/\eta$, and $D=(k/\eta)^{1/3}d_\beta$. The various regimes are the first Hall-resistive (HRi), second Hall-resistive (HRii), first semicollisional (SCi), second semicollisional (SCii), first resistive-inertial (RIi), second resistive-inertial (RIii), first visco-resistive (VRi), second visco-resistive (VRii), visco-inertial (VI), and inertial (I).

G. Summary

The various linear drift-MHD response regimes for a static error field are listed in Table I. By replacing p with p_* in all of the validity criteria listed above, it is possible to determine the extents of these response regimes in Q–P space—the results are illustrated in Figs. 1–3. It can be seen that as the drift parameter, D, increases, the familiar MHD, constant-ψ response regimes (modified by diamagnetism)—i.e., the RI and VR regimes[8]—are gradually replaced by completely new drift-MHD, constant-ψ regimes—i.e., the HR and SC regimes. Note that the reconnecting layer width falls below d_β (which is equivalent to ρ_s in a low-β plasma) in both these new regimes.

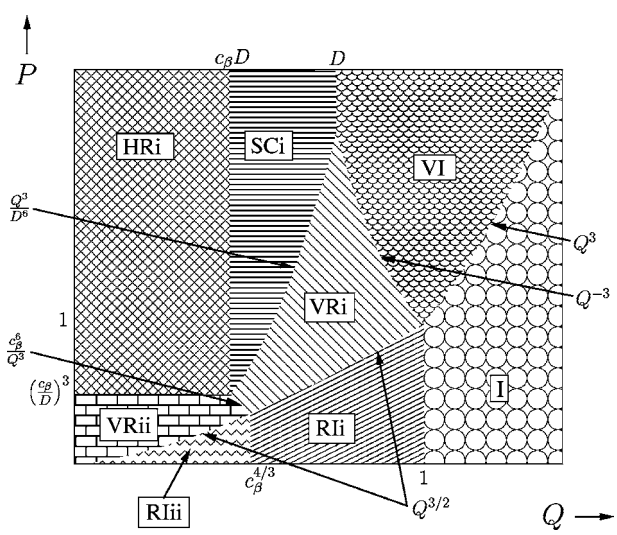

FIG. 1. A schematic diagram of the linear drift-MHD response regimes in Q–P space for the case $D\ll c_\beta^{1/3}$. Here, $Q=(k/\eta)^{1/3}V$, $P=\mu_i/\eta$, and $D=(k/\eta)^{1/3}d_\beta$. The various regimes are the first Hall-resistive (HRi), first semicollisional (SCi), first resistive-inertial (RIi), second resistive-inertial (RIii), first visco-resistive (VRi), second visco-resistive (VRii), visco-inertial (VI), and inertial (I).

IV. APPLICATION TO TOKAMAKS

A. Introduction

In this section, we shall discuss the application of the slab analysis presented in the preceding sections to the problem of determining the error-field penetration threshold in a large aspect ratio, low beta, ohmically heated, tokamak plasma. In the following, we shall assume that $\tau\equiv T_i/T_e=0$, for the sake of simplicity. This implies that $V_{*i}=0$ and V_{*e}

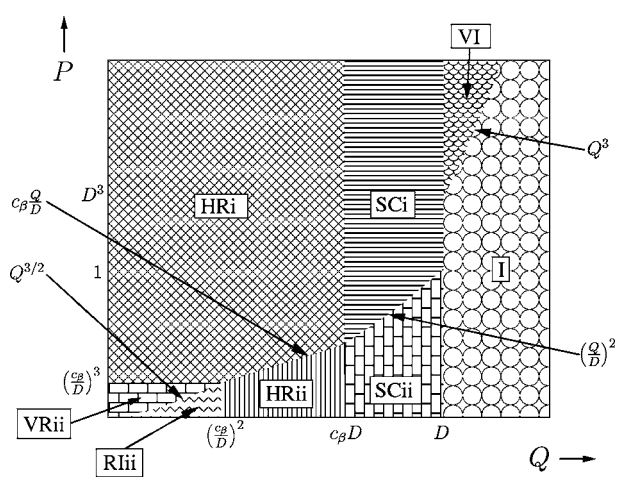

FIG. 3. A schematic diagram of the linear drift-MHD response regimes in Q–P space for the case $D\gg 1$. Here, $Q=(k/\eta)^{1/3}V$, $P=\mu_i/\eta$, and $D=(k/\eta)^{1/3}d_\beta$. The various regimes are the first Hall-resistive (HRi), second Hall-resistive (HRii), first semicollisional (SCi), second semicollisional (SCii), second resistive-inertial (RIii), second visco-resistive (VRii), visco-inertial (VI), and inertial (I).

$=-V_*$. Note, however, that none of the results obtained in this section would change radically were τ nonzero.

Consider a large aspect ratio, low beta, tokamak plasma with approximately circular flux surfaces. Let R_0 and a be the major and minor radii of the plasma, respectively. To a good approximation, the plasma can be treated as a periodic cylinder with period $2\pi R_0$. Adopting standard cylindrical coordinates, (r,θ,z), and simulated toroidal coordinates, (r,θ,ϕ), where $\phi=z/R_0$, the equilibrium magnetic field takes the form $[0,B_\theta(r),B_\phi]$, where B_ϕ plays the role of the guide field. Suppose that the error field is helical, with m periods in the poloidal direction, and n periods in the toroidal direction. The error field resonates with the plasma at the rational flux surface, radius r_s, where $mB_\theta(r_s)/r_s-nB_\phi/R_0=0$.

It is convenient to specify the scale length, scale magnetic field strength, and scale time introduced in Sec. II A as follows: $l=r_s$, $B_l=s(r_s)B_\theta(r_s)$, $t_l=m\tau_H$. Here, $s(r)=(d\ln q/d\ln r)_{r_s}$ is the magnetic shear at the rational surface, and $q(r)=rB_\phi/R_0B_\theta(r)$ is the safety-factor profile. The characteristic hydromagnetic, resistive, and viscous time scales are defined: $\tau_H=R_0\sqrt{\mu_0\rho(r_s)}/[ns(r_s)B_\phi]$, $\tau_R=\mu_0 r_s^2/\eta(r_s)$, and $\tau_V=r_s^2\rho(r_s)/\mu(r_s)$, respectively. Here, ρ is the plasma mass density. Finally, the Lundquist and magnetic Prandtl numbers take the form: $S=\tau_R/\tau_H$, and $P=\tau_R/\tau_V$, respectively.

Using the above definitions, we can identify the following correspondences between slab and tokamak quantities: $k/\eta\rightarrow S$, $k/\mu\rightarrow S/P$, $V\rightarrow\omega\tau_H$, $V_0\rightarrow\omega_0\tau_H$, $V_*\rightarrow\omega_*\tau_H$. Here, ω is the (angular) oscillation frequency of an m,n mode comoving with the $\mathbf{E}\times\mathbf{B}$ frame at the rational surface (as seen in the lab frame), ω_0 is the value of ω in the absence of an error field, and ω_* is the electron diamagnetic frequency at the rational surface. Furthermore, the parameter β is the conventional plasma beta evaluated at the rational surface (taking $\Gamma=1$, for the sake of simplicity). Finally, given that $\beta\ll 1$, the parameter d_β reduces to $\rho_s(r_s)/r_s$, where ρ_s is the ion Larmor radius calculated using the electron temperature.

We also have $Q\rightarrow S^{1/3}\omega\tau_H$, $Q_0\rightarrow S^{1/3}\omega_0\tau_H$, $Q_i\rightarrow 0$, $Q_e\rightarrow S^{1/3}\omega_*\tau_H$, $D\rightarrow S^{1/3}\rho_s/r_s$, $\alpha\rightarrow S^{-1/3}(-r_s\Delta_s')$, and $\xi\rightarrow S^{1/2}[2/s(r_s)][b_r(r_s)/B_\theta(r_s)]$. Here, Δ_s' is the conventional tearing stability index of the m,n mode, and $b_r(r)$ the vacuum radial magnetic perturbation associated with the error field (i.e., the magnetic perturbation in the absence of plasma).

B. Torque balance

The slab force balance equation (16) is transformed into the following toroidal torque balance equation:[7,8]

$$\frac{\mathrm{Im}[\hat{\Delta}(Q)]}{|\alpha+\hat{\Delta}(Q)|^2}=\frac{4P(Q_0-Q)}{\kappa\xi^2}. \tag{59}$$

Here,

$$\kappa=2\int_{r_s}^{a}\frac{\mu(r_s)}{\mu(r)}\frac{dr}{r}\left[\frac{B_\theta(r_s)}{B_\phi}\right]^2 \tag{60}$$

is a slab-to-tokamak correction factor. This factor arises, first, because the global viscous diffusion equation has slightly different forms in slab and cylindrical geometry, and, second, because a tokamak plasma is subject to strong poloidal flow damping which effectively eliminates the poloidal contributions to the mode frequency and electromagnetic torque, leaving the much smaller toroidal contributions.[7,8] It is convenient to rewrite the torque balance equation as

$$\frac{\mathrm{Im}[\hat{\Delta}(Q)]}{|\alpha+\hat{\Delta}(Q)|^2}=\frac{2P(Q_0-Q)}{S\hat{\kappa}[b_r(r_s)/B_\phi]^2}, \tag{61}$$

where $\hat{\kappa}=[2/s(r_s)]^2\int_{r_s}^{a}[\mu(r_s)/\mu(r)](dr/r)$.

C. Error-field penetration thresholds

We generally expect $S\gg 1$ in a high temperature tokamak plasma. Moreover, $|r_s\Delta_s'|\sim O(1)$, assuming that the plasma m,n mode is a (stable) tearing mode. It therefore follows that $\alpha\equiv S^{-1/3}(-r_s\Delta_s')\ll 1$. Hence, it is a good approximation to neglect α in the above torque balance equation. The error-field penetration threshold corresponds to the critical error-field amplitude above which torque balance is lost, i.e., the approximated torque balance equation has no solution.[7,8] It follows that

$$\left[\frac{b_r(r_s)}{B_\phi}\right]^2_{\mathrm{crit}}=\max\left[\frac{2P(Q_0-Q)}{S\hat{\kappa}\,\mathrm{Im}[-\hat{\Delta}(Q)^{-1}]}\right], \tag{62}$$

where the maximum is obtained by varying Q.

D. Penetration thresholds in ohmic tokamak plasmas due to E×B rotation

Suppose that the natural rotation of the m,n mode is entirely due to $\mathbf{E}\times\mathbf{B}$ rotation at the rational surface (i.e., there is no diamagnetic component). This implies that $\omega_*=0$. Now, we do not expect the flow in an ohmically heated tokamak plasma to be sufficiently large that the error-field response regime violates the constant-ψ approximation.[7,8] We also expect that $P>1$.[7,8] It follows, from Sec. III G, that the three most likely error-field response regimes are the first visco-resistive (VRi) regime, the first semicollisional (SCi) regime, and the first Hall-resistive (HRi) regime—see Table I. According to Fig. 2, the VRi regime holds when $D^2P^{1/3}<Q$, the SCi regime holds when $c_\beta D<Q<D^2P^{1/3}$, and the HRi regime holds when $Q<c_\beta D$.

It follows, from Table I and Eq. (62), that error-field penetration occurs in the VRi regime when the natural mode rotation frequency is reduced to 1/2 of its original value, and

$$\left[\frac{b_r(r_s)}{B_\phi}\right]_{\mathrm{crit,VRi}}=\frac{1.03}{\hat{\kappa}^{1/2}}(\omega_0\tau_H)S^{-1/6}P^{7/12}. \tag{63}$$

This regime is valid provided $(\rho_s/r_s)^2S^{1/3}P^{1/3}<\omega_0\tau_H$.

Error-field penetration occurs in the SCi regime when the natural mode rotation frequency is reduced to 3/5 of its original value, and

$$\left[\frac{b_r(r_s)}{B_\phi}\right]_{\rm crit,SCi} = \frac{1.29}{\hat{\kappa}^{1/2}}(\omega_0\tau_H)^{5/4}S^{-1/4}P^{1/2}(\rho_s/r_s)^{-1/2}. \quad (64)$$

This regime is valid provided $\sqrt{\beta}(\rho_s/r_s) < \omega_0\tau_H < (\rho_s/r_s)^2 S^{1/3}P^{1/3}$.

Finally, error-field penetration occurs in the HRi regime when the natural mode rotation frequency is reduced to 1/2 of its original value, and

$$\left[\frac{b_r(r_s)}{B_\phi}\right]_{\rm crit,HRi} = \frac{1.03}{\hat{\kappa}^{1/2}}(\omega_0\tau_H)S^{-1/4}P^{1/2}(\rho_s/r_s)^{-1/4}\beta^{1/8}. \quad (65)$$

This regime is valid provided $\omega_0\tau_H < \sqrt{\beta}(\rho_s/r_s)$.

E. Penetration thresholds in ohmic tokamak plasmas due to diamagnetic rotation

Suppose, as is somewhat more realistic, that the natural rotation of the m,n mode is entirely due to diamagnetic rotation at the rational surface (i.e., there is no $\mathbf{E}\times\mathbf{B}$ component). This implies that $\omega_0=0$.

It follows, from Table I and Eq. (62), that error-field penetration occurs in the VRi regime when the natural mode rotation frequency is reduced to 7/12 of its original value, and

$$\left[\frac{b_r(r_s)}{B_\phi}\right]_{\rm crit,VRi} = \frac{1.11}{\hat{\kappa}^{1/2}}(\omega_*\tau_H)S^{-1/6}P^{7/12}. \quad (66)$$

This regime is valid provided $(\rho_s/r_s)^2 S^{1/3}P^{1/3} < \omega_*\tau_H$.

Error-field penetration occurs in the SCi regime, when the natural mode rotation frequency is reduced to 3/5 of its original value, and

$$\left[\frac{b_r(r_s)}{B_\phi}\right]_{\rm crit,SCi} = \frac{1.29}{\hat{\kappa}^{1/2}}(\omega_*\tau_H)^{5/4}S^{-1/4}P^{1/2}(\rho_s/r_s)^{-1/2}. \quad (67)$$

This regime is valid provided $\sqrt{\beta}(\rho_s/r_s) < \omega_*\tau_H < (\rho_s/r_s)^2 S^{1/3}P^{1/3}$.

Finally, error-field penetration occurs in the HRi regime when the natural mode rotation frequency is reduced to 1/2 of its original value, and

$$\left[\frac{b_r(r_s)}{B_\phi}\right]_{\rm crit,HRi} = \frac{1.03}{\hat{\kappa}^{1/2}}(\omega_*\tau_H)S^{-1/4}P^{1/2}(\rho_s/r_s)^{-1/4}\beta^{1/8}. \quad (68)$$

This regime is valid provided $\omega_*\tau_H < \sqrt{\beta}(\rho_s/r_s)$.

It can be seen, by comparing the results of this section with those of the preceding one, that it makes little difference to the penetration threshold whether the natural mode frequency is due to $\mathbf{E}\times\mathbf{B}$ or diamagnetic rotation. Hence, in the following, we shall employ the expressions for the penetration threshold occurring in Sec. IV D, with the understanding that the natural frequency, ω_0, represents the unperturbed mode frequency at the rational surface, and can be made up of both diamagnetic and $\mathbf{E}\times\mathbf{B}$ components.

F. Scaling of ohmic penetration thresholds

The parameters appearing in Eqs. (63)–(65) are not directly measurable in tokamak experiments. However, we can easily express them in terms of the standard dimensionless parameters: $\rho_* \equiv \rho_s/R_0 \sim T_e^{1/2}/(R_0 B_\phi)$, $\beta \sim n_e T_e/B_\phi^2$, and $\nu_* \sim n_e R_0/T_e^2$. Here, T_e is the electron temperature. The collisionality parameter ν_* is the ratio of the typical electron-ion collision frequency to the transit frequency (i.e., the number of times per second a typical electron executes a toroidal circuit of the plasma). The parameters appearing in Eqs. (63)–(65) can also be expressed in terms of the engineering parameters: n_e, T_e, B_ϕ, and R_0.

Consider a class of ohmically heated tokamak plasmas in which the aspect ratio, R_0/a, and the equilibrium profiles are held fixed. By definition, $\omega_*\tau_H \sim T_e\sqrt{n_e}/(R_0 B_\phi^2)$, $S \sim B_\phi T_e^{3/2}R_0/\sqrt{n_e}$, and $P \sim R_0^2 T_e^{3/2}/\tau_M$. Here, the parallel resistivity is assumed to obey the classical Spitzer formula, and τ_M is the momentum confinement time. It immediately follows, by inspection of the various powers of T_e, B_ϕ, etc., that $\omega_*\tau_H \sim \beta^{1/2}\rho_*$, $S \sim \beta^{1/2}/(\nu_*\rho_*^2)$, and $P \sim \beta/(B_\phi\tau_M\nu_*\rho_*^3)$.

Let us assume, as seems plausible, that the natural mode frequency, ω_0, scales like the diamagnetic frequency, ω_*. We shall also assume, with considerably less justification, that the momentum confinement time, τ_M, scales like the energy confinement time, τ_E.[7] For an ohmically heated tokamak, we can balance the ohmic heating rate against the energy loss rate. It follows that $B_\phi\tau_E \sim B_\phi\tau_M \sim \rho_*^{-3}\nu_*^{-1}\beta^2$. This relation can be used to eliminate τ_M from $P \sim \beta/(B_\phi\tau_M\nu_*\rho_*^3)$, yielding $P \sim \beta^{-1}$.

In terms of dimensionless parameters, the error-field penetration threshold is found to scale as

$$\left[\frac{b_r(r_s)}{B_\phi}\right]_{\rm crit,VRi} \sim \rho_*^{4/3}\nu_*^{1/6}\beta^{-1/6}, \quad (69)$$

$$\left[\frac{b_r(r_s)}{B_\phi}\right]_{\rm crit,SCi} \sim \rho_*^{5/4}\nu_*^{1/4}, \quad (70)$$

$$\left[\frac{b_r(r_s)}{B_\phi}\right]_{\rm crit,HRi} \sim \rho_*^{5/4}\nu_*^{1/4}, \quad (71)$$

in the first visco-resistive, first semicollisional, and first Hall-resistive regimes, respectively.

In terms of engineering parameters, the penetration threshold is found to scale as

$$\left[\frac{b_r(r_s)}{B_\phi}\right]_{\rm crit,VRi} \sim T_e^{1/6}B_\phi^{-1}R_0^{-7/6}, \quad (72)$$

$$\left[\frac{b_r(r_s)}{B_\phi}\right]_{\rm crit,SCi} \sim n_e^{1/4}T_e^{1/8}B_\phi^{-5/4}R_0^{-1}, \quad (73)$$

$$\left[\frac{b_r(r_s)}{B_\phi}\right]_{\rm crit,HRi} \sim n_e^{1/4}T_e^{1/8}B_\phi^{-5/4}R_0^{-1}. \quad (74)$$

As is easily demonstrated, the theoretical scaling of the penetration threshold with engineering parameters is of the general form $[b_r(r_s)/B_\phi]_{\rm crit} \sim n_e^{\alpha_n}T_e^{\alpha_T}B_\phi^{\alpha_B}R_0^{\alpha_R}$, where $\alpha_R = 2\alpha_n + 0.5\alpha_T + 1.25\alpha_B$.

Experimentally,[6] the error-field penetration threshold is found to increase approximately linearly with electron number density. The above scalings, which are all fairly similar to one another, exhibit a significantly weaker than linear increase with electron number density (unless T_e increases very rapidly with increasing n_e). The theoretical scalings also exhibit a fairly strong, approximately linear decrease with increasing toroidal magnetic field strength. This scaling is consistent with experimental data obtained from DIII-D, JET, and Alcator C-Mod.[6] The scaling of the penetration threshold with the plasma major radius is not directly measured in experiments, but is, instead, inferred from the observed scalings with electron density and toroidal magnetic field strength via dimensional analysis. Hence, if there is agreement between prediction and experiment on the scaling of the penetration threshold with electron number density and toroidal magnetic field strength, then there will also be agreement on the scaling with plasma major radius. Unfortunately, the predicted and experimental scalings of the penetration threshold with the electron number density are in disagreement.

V. SUMMARY

The MHD model of error-field penetration in tokamak plasmas presented in Refs. 7–9 has been extended to take drift-MHD physics into account. Diamagnetic and semicollisional (i.e., the layer width falling below ρ_s) effects are both found to modify the penetration threshold. However, these modifications are not particularly dramatic.[12]

The extended model has been used to examine the scaling of the error-field penetration threshold in ohmic tokamak plasmas. In order to perform a scaling study, it is necessary to make some assumptions regarding the scaling of the natural frequency of tearing modes in the plasma, and that of the plasma momentum confinement time scale. The scaling of the penetration threshold thus obtained is found to be fairly close to that previously obtained from MHD.[8] In general, the predicted scalings are not entirely in accordance with the scaling of the penetration threshold measured in experiments. The predicted scalings generally exhibit too slow an increase of the penetration threshold with increasing electron number density, but about the right decrease with increasing toroidal magnetic field strength.

The lack of agreement between the predicted and experimental penetration threshold scalings may be due to incorrect assumptions regarding the scalings of the natural mode frequency and the momentum confinement time scale. Alternately, this lack of agreement may indicate that more physics needs to be added to the model. For instance, neoclassical flow-damping is known to give rise to a large enhancement of ion inertia.[18] Such an enhancement would shift the boundaries of the various linear response regimes (see the figures), which could modify the penetration threshold. Neoclassical effects also allow nonresonant components of an error field to exert a slowing-down torque on the plasma, thus affecting the penetration threshold.[19] Both these effects will be investigated in future publications.

ACKNOWLEDGMENTS

The authors would like to thank Steve Wolfe and Rob La Haye for helpful discussions during the preparation of this paper. One of the authors (A.C.) would also like to acknowledge helpful discussions with Boris Breizman.

This research was funded by the U.S. Department of Energy under Contract DE-FG05-96ER-54 346.

[1] J. T. Scoville, R. J. La Haye, A. G. Kellman, T. H. Osborne, R. D. Stambaugh, E. J. Strait, and T. S. Taylor, Nucl. Fusion **31**, 875 (1991).
[2] T. C. Hender, R. Fitzpatrick, A. W. Morris, P. G. Carolan, R. D. Durst, T. Edlington, J. Ferreira, S. J. Fielding, P. S. Haynes, J. Hugill, I. J. Jenkins, R. J. La Haye, B. J. Parham, D. C. Robinson, T. N. Todd, M. Valovič, and G. Vayakis, Nucl. Fusion **32**, 2091 (1992).
[3] G. M. Fishpool and P. S. Haynes, Nucl. Fusion **34**, 109 (1994).
[4] R. J. Buttery, M. De Benedetti, D. A. Gates, Y. Gribov, T. C. Hender, R. J. La Haye, P. Leahy, J. A. Leuer, A. W. Morris, A. Santagiustina, J. T. Scoville, and B. J. D. Tubbing, JET Team, COMPASS-D Research Team, DIII-D Team, Nucl. Fusion **39**, 1827 (1999).
[5] R. J. Buttery, M. De Benedetti, T. C. Hender, and B. J. D. Tubbing, Nucl. Fusion **40**, 807 (2000).
[6] S. M. Wolfe, I. R. Hutchinson, R. S. Granetz, J. Rice, A. Hubbard, A. Lynn, P. Phillips, T. C. Hender, D. F. Howell, R. J. La Haye, and J. T. Scoville, Phys. Plasmas **12**, 056 110 (2005).
[7] R. Fitzpatrick, Nucl. Fusion **33**, 1049 (1993).
[8] R. Fitzpatrick, Phys. Plasmas **5**, 3325 (1998).
[9] R. Fitzpatrick, Phys. Plasmas **10**, 1782 (2003).
[10] R. D. Hazeltine and J. D. Meiss, *Plasma Confinement* (Dover, Mineola, NY, 2003).
[11] J. F. Drake and Y. C. Lee, Phys. Fluids **20**, 1341 (1976).
[12] F. L. Waelbroeck, Phys. Plasmas **10**, 4040 (2003).
[13] R. Fitzpatrick and F. L. Waelbroeck, Phys. Plasmas **12**, 022 307 (2005).
[14] H. P. Furth, J. Killeen, and M. N. Rosenbluth, Phys. Fluids **6**, 459 (1963).
[15] A. Erdelyi, W. Magnus, F. Oberhettinger, and F. G. Tricomi, *Higher Transcendental Functions* (McGraw-Hill, New York, 1953), Vol. II.
[16] G. Ara, B. Basu, B. Coppi, G. Laval, M. N. Rosenbluth, and B. V. Waddell, Ann. Phys. **212**, 443 (1978).
[17] A. H. Boozer, Phys. Plasmas **3**, 4620 (1996).
[18] A. B. Mikhailovskii and B. N. Kuvshinov, Plasma Phys. Rep. **21**, 789 (1995).
[19] E. Lazzaro, R. J. Buttery, T. C. Hender *et al.*, Phys. Plasmas **9**, 3906 (2002).